

Identification of novel STAT3 inhibitors bearing 2-acetyl-7-phenylamino benzofuran scaffold for antitumour study

Feng Wang, Kai-Rui Feng, Jia-Ying Zhao, Jian-Wei Zhang, Xin-Wei Shi, Jian Zhou, Dingding Gao, Guo-Qiang Lin, Ping Tian

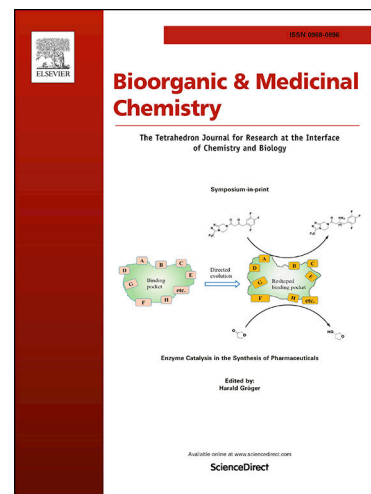
PII: S0968-0896(20)30652-0
DOI: <https://doi.org/10.1016/j.bmc.2020.115822>
Reference: BMC 115822

To appear in: *Bioorganic & Medicinal Chemistry*

Received Date: 28 July 2020
Revised Date: 9 October 2020
Accepted Date: 13 October 2020

Please cite this article as: F. Wang, K-R. Feng, J-Y. Zhao, J-W. Zhang, X-W. Shi, J. Zhou, D. Gao, G-Q. Lin, P. Tian, Identification of novel STAT3 inhibitors bearing 2-acetyl-7-phenylamino benzofuran scaffold for antitumour study, *Bioorganic & Medicinal Chemistry* (2020), doi: <https://doi.org/10.1016/j.bmc.2020.115822>

This is a PDF file of an article that has undergone enhancements after acceptance, such as the addition of a cover page and metadata, and formatting for readability, but it is not yet the definitive version of record. This version will undergo additional copyediting, typesetting and review before it is published in its final form, but we are providing this version to give early visibility of the article. Please note that, during the production process, errors may be discovered which could affect the content, and all legal disclaimers that apply to the journal pertain.



Identification of novel STAT3 inhibitors bearing 2-acetyl-7-phenylamino benzofuran scaffold for antitumour study

Feng Wang ^{a, #}, Kai-Rui Feng ^{a, #}, Jia-Ying Zhao ^a, Jian-Wei Zhang ^a, Xin-Wei Shi ^a, Jian Zhou ^{b, *}, Dingding Gao ^{a, b, *}, Guo-Qiang Lin ^{a, c}, and Ping Tian ^{a, c, *}

^a *The Research Center of Chiral Drugs, Innovation Research Institute of Traditional Chinese Medicine, Shanghai University of Traditional Chinese Medicine, Shanghai 201203, China*

^b *Shanghai Engineering Research Center of Molecular Therapeutics and New Drug Development; School of Chemistry and Molecular Engineering, East China Normal University, 3663N Zhongshan Road, Shanghai 200062, China*

^c *CAS Key Laboratory of Synthetic Chemistry of Natural Substances, Center for Excellence in Molecular Synthesis, Shanghai Institute of Organic Chemistry, University of Chinese Academy of Sciences, Chinese Academy of Sciences, Shanghai 200032, China*

[#] These authors contributed equally to this work.

^{*} Corresponding authors:

E-mail addresses: gaodingding@shutcm.edu.cn (Dingding Gao), jzhou@chem.ecnu.edu.cn (Jian Zhou), tianping@shutcm.edu.cn or tianping@sioc.ac.cn (Ping Tian)

ABSTRACT

Signal transducer and activator of transcription 3 (STAT3) is identified as a promising target for multiple cancer therapy and attracts widespread concern. Herein, we reported the discovery of a series of 2-acetyl-7-phenylamino benzofuran derivatives as STAT3 inhibitors using scaffold fusion strategy. Further structure activity relationship study led to the discovery of compound **C6**, which displayed the most potent anti-proliferation activities against MDA-MB-468 cells ($IC_{50} = 0.16 \mu M$). Western blot assay demonstrated that **C6** inhibited the activation of STAT3 (Tyr705) without influencing the phosphorylation of STAT1 (Tyr701). Further mechanistic studies indicated that **C6** caused a notable G2/M cycle-arresting and early apoptosis in a concentration-dependent manner in MDA-MB-468 cells. Finally, molecular modelling study elucidated the binding mode of **C6** in STAT3 SH2 domain.

Keywords: STAT3 inhibitors, 2-Acetyl-7-phenylamino benzofurans, Structure-activity relationships, Antitumor study, Molecular docking

1. Introduction

Signal transducer and activator of transcription 3 (STAT3) belongs to the STAT protein family that regulates a diverse array of cellular events.¹⁻³ In response to a variety of extracellular cytokines (IL-6, IL-11, LIF, CNTF, OSM, and IL-31, etc.) and growth factors (EGF, FGF, and PDGF, etc.), the activation of STAT3 is phosphorylated at Tyr705 residue by the receptor or non-receptor tyrosine kinases, G-protein-coupled receptors (GPCRs) and Toll-like receptors (TLRs).⁴⁻⁶ Phosphorylated STAT3 (p-STAT3) proteins form homodimerization, then translocate to the nucleus, bind to the specific promoters of genes and induce a genetic programme that promotes various cellular processes.⁷⁻⁹ In normal cells, the duration of STAT3 activation is transient, but in those with haematopoietic malignancies or solid tumours, such as breast, colorectal, ovarian, lung and pancreatic, the STAT3 signalling pathway is aberrantly hyperactivated, which can promote tumour cell proliferation, survival, invasiveness, and metastasis.¹⁰⁻¹³ STAT3 not only acts as a direct transcription factor, but also regulates gene expression through epigenetic mechanisms, such as DNA methylation and chromatin modulation.⁶ Multiple studies have been proved that the activated STAT3 plays an important role in immunosuppressive regulation in immune cells and tumour-infiltrating immune cells, which can negatively regulate neutrophils, natural killer cells, effector T cells, and dendritic cells while positively regulating populations of myeloid-derived suppressor cells and regulatory T cells.¹⁴⁻¹⁶ What's more, the hyperactivation STAT3 signalling is often associated with poor patient outcomes in the pathogenesis of cancer.¹⁷⁻¹⁹ Therefore, the STAT3 signaling pathway is an attractive target for cancer therapy and the development of selective, potent STAT3 inhibitors is highly desirable.

During the past few years, abundant efforts have been made to develop effective STAT3 inhibitors and accomplished remarkable progress.^{20,21} In general, the strategies of inhibiting STAT3 signalling pathway mainly include directly targeting STAT3 protein and indirectly targeting upstream kinases. However, due to the challenge of selectivity and drug resistance for kinases inhibitors, directly targeting STAT3 protein

exhibits unique advantages. To our knowledge, the advantages of STAT3 inhibitors for cancer therapy are as follows: (1) Blocking STAT3 signalling pathway is sufficient to induce growth arrest and apoptosis in many different tumor types despite multiple oncogenic signalling pathways can be operative in a single tumor; (2) Compared to many different upstream tyrosine kinases of STAT protein, there are only two STAT proteins (STAT3 and STAT5) frequently activated in human cancers; (3) Compared to tyrosine kinases inhibitors, direct STAT3 inhibitors have good selectivity and can overcome cytokine-mediated drug resistance. Some representative STAT3 inhibitors are listed in Fig. 1, such as **1** (BBI608), **2**, **3** (LY-5), **4** (Stattic), **5** (LLL-12), **6** (STA-21), **7** (Niclosamide), **8** (HJC0146).²²⁻²⁹ Unfortunately, effective STAT3 inhibitors that can generate potent antitumour effects in the clinic remain to be further explored.

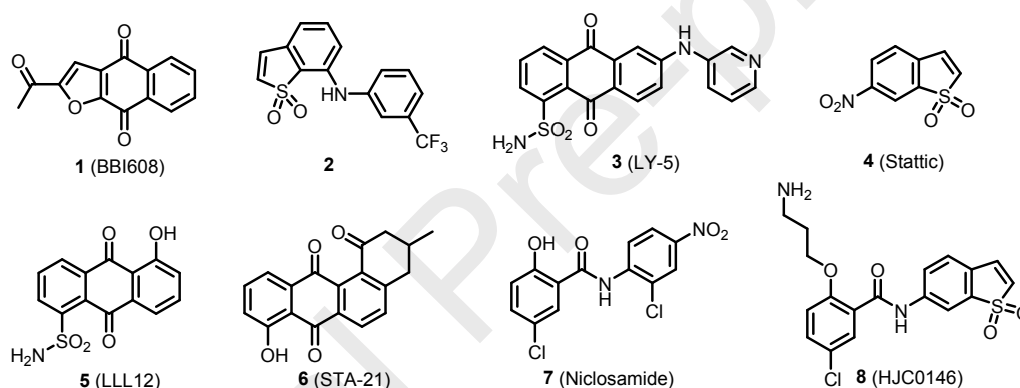


Fig. 1. Representative small-molecule STAT3 inhibitors.

Among all the reported small molecular STAT3 inhibitors, BBI608 (Napabucasin) is in the highest clinical stage for cancer therapy.³⁰ Molecular docking studies show that it targets the STAT3 SH2 domain and the 2-acetylfuran group is located at the pY705 site (also named pY+0 site), and leaves the pY+X site cavity unoccupied (Fig. 2A). In 2017, Kong and co-workers reported a series of STAT3 inhibitors with benzo[b]thiophene 1,1-dioxide scaffold and compound **2** demonstrated the most potent inhibitory activity.²³ Further docking study indicated that the 3-(trifluoromethyl)aniline group is binding at the pY+X site (Fig. 2B). Accordingly, using scaffold fusion strategy, novel STAT3 inhibitors with 2-acetyl-7-phenylamino benzofuran scaffold was designed to occupy both the pY705 and pY+X sites. Subsequently, the structure-activity relationship was explored to obtain more potential STAT3 inhibitors. (Fig.3)

Particularly, compound **C6** displayed the most potent anti-proliferation activities against MDA-MB-468 cells with an IC_{50} value of $0.16 \pm 0.01 \mu M$. Further mechanistic study based on **C6** was also conducted and investigated.

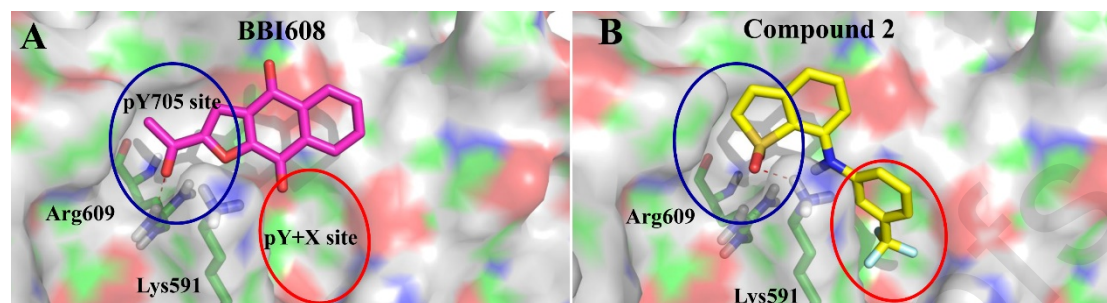


Fig. 2. Molecular docking study of compound BBI608 and compound 2.

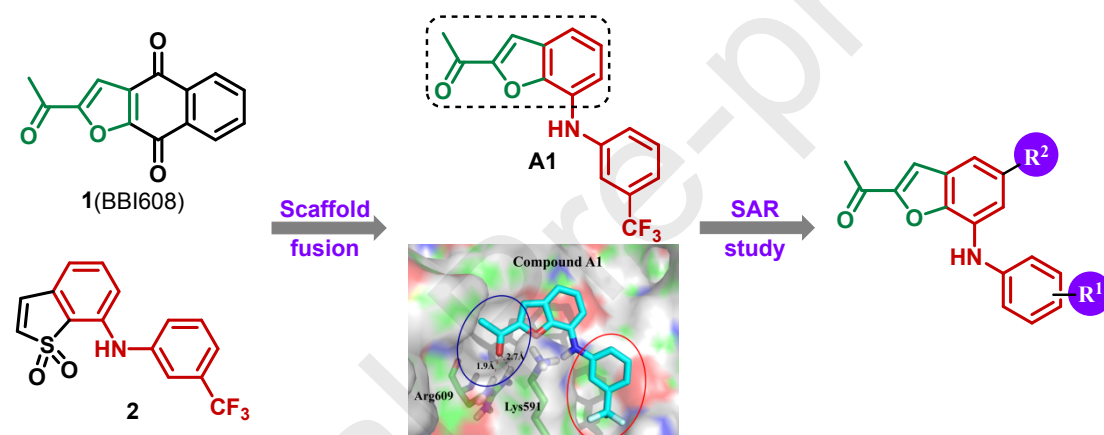


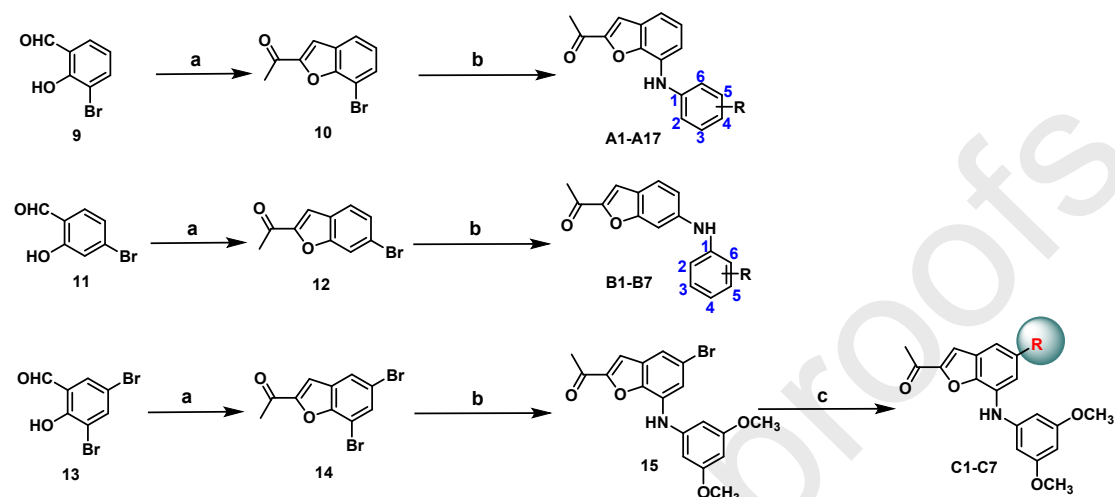
Fig. 3. Structure-based design of STAT3 inhibitors by scaffold fusion and SAR study.

2. Results and discussion

2.1. Chemistry

The synthetic routes for the preparation of the target compounds **A1-A17**, **B1-B7** and **C1-C7** were outlined in Scheme 1. Commercially available salicylaldehyde derivatives **9**, **11** and **13** were used as the starting material for the preparation of intermediates **10**, **12**, and **14** respectively using bromoacetone, which underwent a cyclization reaction.³¹ Then, Pd-catalyzed C-N cross-coupling reaction was carried out by reacting with multiple phenylamine derivatives to afford compounds **A1-A17**, **B1-B7** and **15**.³² Compounds **C1-C6** was prepared via a classic C-C Suzuki coupling reaction of boronic acid derivative with the key intermediate **15**.³³ However, a copper-catalyzed

homocoupling reaction was conducted by mixing morpholine and compound **15** to obtain designed compound **C7**.³⁴ Importantly, a representative compound **C6** was unequivocally established by an X-ray crystal structure (CCDC 2018188) to validated the correct structures of series-C compounds (Fig. 4).³⁵



Scheme 1. Reagents and conditions: (a) $\text{BrCH}_2\text{COCH}_3$, Cs_2CO_3 , DMF, 0 °C to 60 °C, 8 h; (b) corresponding aniline derivatives, $\text{Pd}(\text{OAc})_2$, Cs_2CO_3 , BINAP, toluene, 120 °C, 10 h; (c) **C1-C6**: $\text{RB}(\text{OH})_2$, $\text{Pd}(\text{dppf})\text{Cl}_2$, K_2CO_3 , DMF/ H_2O , N_2 , 100 °C, 8h. **C7**: morpholine, K_2CO_3 , CuI, L-proline, DMSO, N_2 , 90 °C, 12 h.

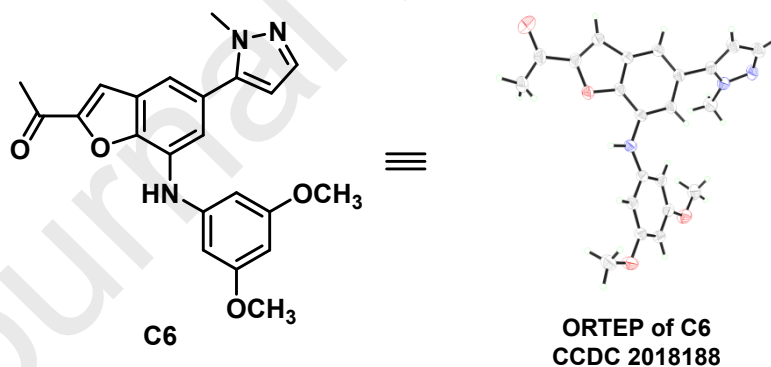


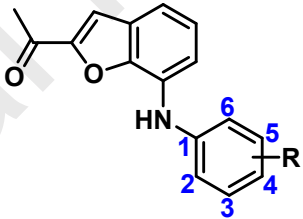
Fig. 4. X-ray crystallography of compound **C6**.

2.2. In vitro anti-proliferation evaluation

According to our design strategy, a total of 17 series-A compounds were firstly synthesized and evaluated with their anti-proliferation activity against MDA-MB-468 cells (STAT3 over-expressed human cancer cell lines) via established CCK-8 assay. BBI608 was used as a reference drug. As shown in table 1, the target compound **A1**

derived from BBI608 and compound **2** displayed moderate inhibitory activity with an IC_{50} value of 4.86 μ M. However, the removal of trifluoromethyl group (**A2**) or changing it to methyl (**A3**) or cyano group (**A7**) led to a significant loss of potency. Replacing the trifluoromethyl group of **A1** to chlorine (**A4**), methoxyl (**A5**) or fluorine (**A6**) slightly increased the inhibitory activity (**A4**: IC_{50} = 3.37 μ M, **A5**: IC_{50} = 1.83 μ M, **A6**: IC_{50} = 2.55 μ M). When the substituent group located at the C4 position of the benzene ring, only trifluoromethyl (**A10**) and methyl (**A8**) displayed potent inhibitory activities with IC_{50} values of 1.90 μ M and 5.53 μ M, respectively. However, compounds **A9** and **A11** with 4-OCH₃ and 4-F lost the activities. Next, we kept the methoxyl at C3 position and introduced additional substituent, such as fluorine (**A12**), methyl (**A13**), chlorine (**A14**), methoxyl (**A15**), hydroxy (**A16**) at C4 position or methoxyl (**A17**) at C5 position. Among them, compound **A17** led to a 3-fold increased potency (IC_{50} = 0.67 μ M), which was better than positive compound BBI608. Unfortunately, the movement of the aniline substituent from C7' (Series-A) to C6' (Series-B) position resulted in a total loss of the antitumor activity (Table 2).

Table 1. Antiproliferative activity of series-A compounds



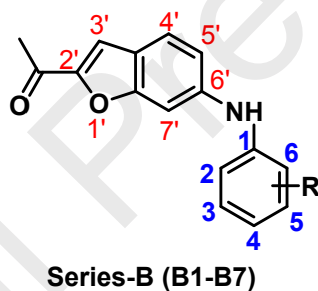
Series-A (A1-A17)

Compd.	R	MDA-MB-468 $IC_{50} \pm SD$ (μ M) ^a
A1	3-CF ₃	4.86 \pm 0.07
A2	H	>25
A3	3-CH ₃	16.3 \pm 0.25
A4	3-Cl	3.37 \pm 0.12
A5	3-OCH ₃	1.83 \pm 0.05
A6	3-F	2.55 \pm 0.11
A7	3-CN	>20
A8	4-CH ₃	5.53 \pm 0.15

A9	4-OCH ₃	>25
A10	4-CF ₃	1.90±0.98
A11	4-F	>25
A12	3-OCH ₃ ,4-F	1.82±0.25
A13	3-OCH ₃ ,4-CH ₃	10.10±0.53
A14	3-OCH ₃ ,4-Cl	8.00±0.91
A15	3-OCH ₃ ,4-OCH ₃	>25
A16	3-OCH ₃ ,4-OH	2.28±0.39
A17	3-OCH ₃ ,5-OCH ₃	0.67±0.08
2	/	4.15±0.02
BBI608	/	1.14±0.04

^a The inhibitory effects of these compounds on the proliferation of cancer cell lines were determined by the CCK8 assay. The data are the mean ± SD from at least three independent experiments.

Table 2. Antiproliferative activity of series-B compounds



Compd.	R	MDA-MB-468 IC ₅₀ ±SD (μM) ^a
B1	3-CF ₃	>25
B2	H	>25
B3	3-CH ₃	>25
B4	4-CF ₃	>25
B5	4-CH ₃	>25
B6	3-CH ₃ ,4-F	>25
B7	3-CH ₃ ,5-F	>25
2	/	4.15±0.02
BBI608	/	1.14±0.04

^a The inhibitory effects of these compounds on the proliferation of cancer cell lines were determined by the CCK8 assay. The data are the mean ± SD from at least three independent experiments.

With these results in hand, we sought to use compound **A17** as a promising starting point, and structural optimization based on molecular docking was carried out to further improve potency. As shown in Fig. 4, there was a big pocket not occupied at the C5' position of 2-acetylbenzofuran core fragment, and bulkier group might be ideally suited to target this region for improving binding affinity. Therefore, a total of seven series-C compounds were designed, synthesized, and evaluated their anti-proliferation activity. As depicted in Table 3, the substitution of phenyl led to a slight drop of activity (**C1**, $IC_{50} = 5.26 \mu M$). Interestingly, the replacement of the phenyl by a five-membered heterocycle moiety, such as thiophene (**C2**), furan (**C4**), and N-methylpyrazole (**C6**) resulted in improved antitumor activities. When the phenyl group was converted to cyclohexenyl (**C3**), 2, 3-dihydropyranyl (**C5**), morpholinyl (**C7**), the antiproliferative activity was dramatically losing. Additionally, we evaluated the anti-proliferation of compound **C6** in different STAT3 over-expressed human cancer cell lines (HepG2, MDA-MB-231, A549, U251, HCT116) to explore its anti-tumor spectrum. As shown in Table 4, **C6** exhibited moderate to good anti-proliferation activities against HepG2, MDA-MB-231 and A549 cancer cell lines with IC_{50} values ranging from $1.63 \mu M$ to $5.80 \mu M$, but was not sensitive to the other two cell lines (U251, HCT116). Taken together, compound **C6** showed the most potent in vitro anti-tumor activity against MDA-MB-468 cell lines ($IC_{50} = 0.16 \mu M$) and was selected for further biological study.

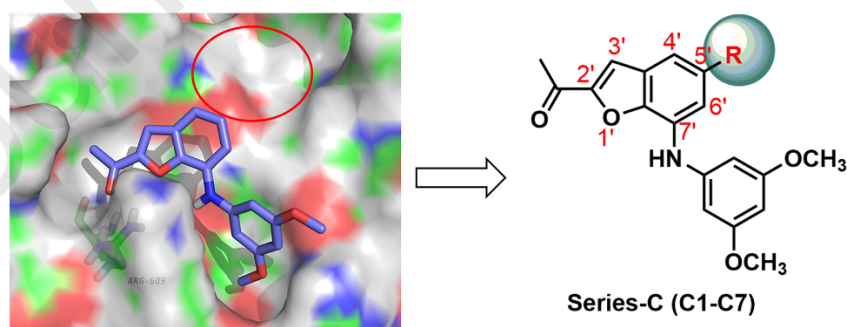
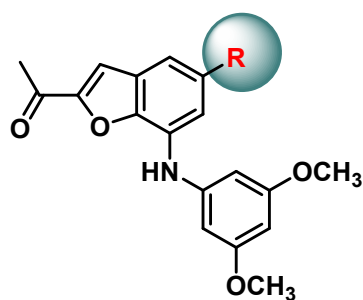


Fig. 4. Structure based design of series-C compounds.

Table 3. Antiproliferative activity of series-C compounds



Compd.	R	MDA-MB-468 IC ₅₀ ±SD (μM) ^a
C1		5.26±0.64
C2		0.63±0.04
C3		NA
C4		0.44±0.02
C5		NA
C6		0.16±0.01
C7		NA
2	/	4.15±0.02
BBI608	/	1.14±0.04

^a The inhibitory effects of these compounds on the proliferation of cancer cell lines were determined by the CCK8 assay. The data are the mean ± SD from at least three independent experiments.

Table 4. Anti-tumor spectrum of compound **C6**

Compd.	MDA-MB-231	HepG2	A549	U251	HCT116
	IC ₅₀ ±SD (μM) ^a	IC ₅₀ ±SD (μM) ^a	IC ₅₀ ±SD (μM) ^a	IC ₅₀ ±SD (μM) ^a	IC ₅₀ ±SD (μM) ^a
C6	5.80±0.66	1.63±0.02	5.73±0.68	>25	>25

^a The inhibitory effects of these compounds on the proliferation of cancer cell lines were determined by the CCK8 assay. The data are the mean ± SD from at least three independent experiments.

2.3. Compounds **C6** inhibited the phosphorylation of *STAT3* and its downstream target

protein C-Myc

The abovementioned SAR study showed that compound **C6** offered highly potent activity against the MDA-MB-468 cell lines. In an attempt to investigate its effect against STAT3 activation (Tyr705) and the downstream target protein (C-Myc), western blot assay was conducted. As shown in Fig. 5, after treating different concentrations of compound **C6** for 24 h, the STAT3 phosphorylation at Tyr705 residue was reduced in a dose-dependent manner without influencing the total STAT3 protein. As we expected, the expression of downstream target protein C-Myc was robustly decreased. STAT1 is another member of STATs family, which was thought to be a tumor suppressor and can inhibit cancer cell proliferation and induce apoptosis. Western blot assay showed that compound **C6** had no effect on the level of STAT1 and its phosphorylation on Tyr701 residue and displayed good selectivity.

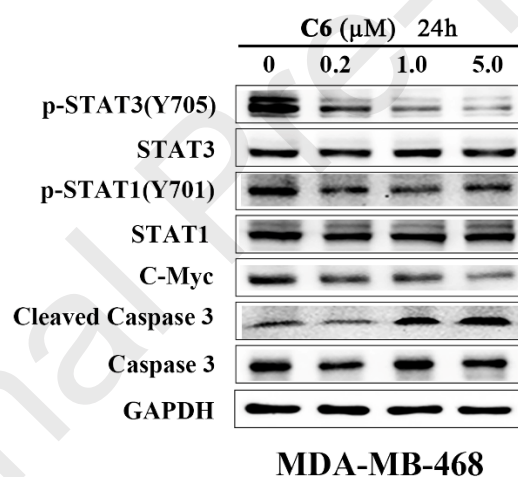


Fig. 5. Western blotting results of compound **C6** in MDA-MB-468 cell lines.

2.4. Compound **C6** induced apoptosis in cancer cells

To investigate the ability of compound **C6** in inducing apoptosis in MDA-MB-468 cells, Annexin-V-FITC/PI staining assay by flow cytometry was performed. As illustrated in Fig. 6, compound **C6** caused significant induction of apoptosis in MDA-MB-468 cells at a low concentration of 1.0 μM and the apoptosis rate was 42.59 %. Particularly, it mainly occurred in early apoptosis. We further explored how compound **C6** induced the apoptosis in MDA-MB-468 cells using western blot assay. As shown in Fig. 5, the protein level of Cleaved Caspases 3, which is a protease of the intrinsic apoptotic

pathway activated in the mitochondrial damage, was increasing in a dose dependent manner after treatment of compound **C6** for 24 h. Thus, we supposed that the manner of compound **C6** inducing apoptosis is mainly through the mitochondrial Caspase dependent apoptotic pathway.

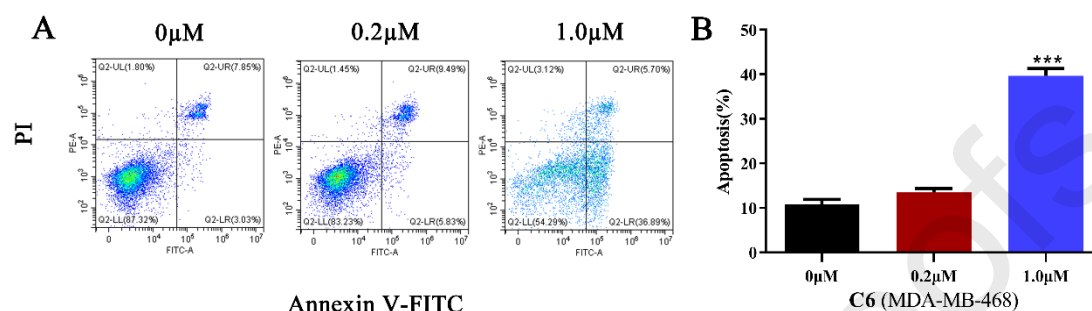


Fig. 6. flow cytometry analysis of the apoptosis induction by compound **C6** in MDA-MB-468 cells.

2.5. Analysis of cell cycle effect

We further analyzed the cell cycle effect of compound **C6** in MDA-MB-468 cells using flow cytometry and an equivalent volume of dimethyl sulfoxide (DMSO) was used as the control. As shown in Fig. 7, the percentage of cells in the G2/M fraction increased from 19.43 to 34.76 and 91.72 %, respectively, after treatment with 0, 0.2 and 1.0 μM compound **C6** for 24 h. These results suggested that **C6** could dose-dependently cause a significant G2/M phase arrest in MDA-MB-468 cells.

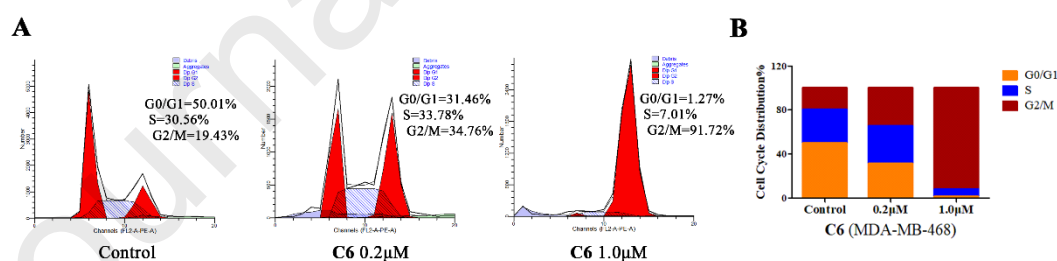


Fig. 7. Cell-cycle arrest analysis of compound **C6** by flow cytometry in MDA-MB-468 cells.

2.6. Molecular docking study

To investigate the binding mode of compound **C6** in the target protein, a docking model of this compound in complex with STAT3 SH2 domain (PDB code 1BG1) was built using Glide module. As depicted in the Fig. 8, the combination pattern of **C6** fit well within the STAT3 SH2 domain and was consistent with our initial expectations. The acetyl group is occupying the important pY705 site and formed a critical hydrogen bond

(1.8 Å) with the guanidine group of Arg609, which was similar to the acetyl group of BBI608. Especially, the 3,5-dimethoxyphenyl in compound **C6** could insert into the side pocket (pY+X site) and generate multiple favorable hydrophobic interactions with the hydrophobic side chain of Ile634, Gln 635, Glu594 residues. Furthermore, the N-methylpyrazole group extended to a large flat region and made favorable van der Waals interactions with Phe621 and Pro639 residues.

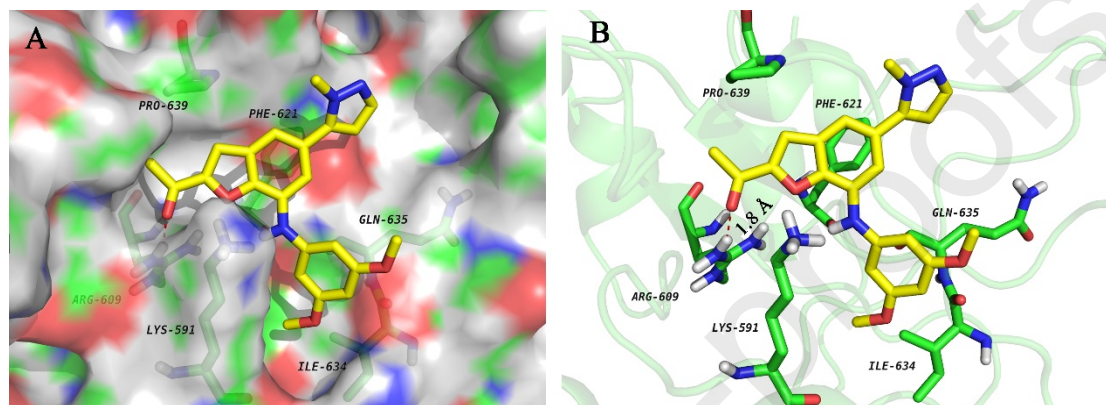


Fig. 8. Predicted binding mode of **C6** in STAT3 SH2 domain (PDB code: 1BG1). (A) **C6** (yellow) bound in the surface of binding site. (B) Predicted interaction of **C6** (yellow) within STAT3 SH2 domain. The figures were generated using Pymol.

3. Conclusions

Taken together, a series of 2-acetyl-7-phenylamino benzofuran derivatives was identified as novel STAT3 inhibitors using scaffold fusion strategy from BBI608 and compound **2**. Further structure optimization and SAR study resulted in the discovery of a highly active and selective STAT3 inhibitor **C6**, which could inhibit the proliferation of MDA-MB-468 cells with an IC_{50} value of $0.16 \pm 0.01 \mu M$. In preliminary mechanistic studies, **C6** reduced the STAT3 phosphorylation at Tyr705 residue in a dose-dependent manner and then downregulated the expression of its downstream protein C-Myc without influencing the activation of STAT1. In addition, molecular docking study elucidated the binding mode of **C6** in STAT3 SH2 domain, which was consistent with our initial expectations. Further pharmaceutical research of compound **C6** are currently underway in our laboratories and will be reported in due course.

4. Experimental section

4.1. Chemistry

Unless otherwise indicated, all solvents and starting materials were purchased from commercial suppliers and used without further purification. All compounds listed in the paper were purified on silica gel (200-300 mesh) using flash chromatography. ^1H NMR and ^{13}C NMR were recorded in CDCl_3 or $\text{DMSO}-d_6$ with Bruker 600 MHz spectrometer at room temperature and Tetramethylsilane (TMS) was used as an internal standard. The NMR data were expressed as follows: chemical shifts (δ , ppm), coupling constants (J , Hz), multiplicity integration (s = singlet, d = doublet, t = triplet, q = quartet, dd = doublet of doublets, m = multiplet). The high-resolution mass spectra (HRMS) was measured on Agilent 6545 Accurate-Mass Q-TOF LC/MS system and MS was detected on Shimadzu 8040 quadrupole. The X-Ray crystal structures of compound **C6** was carried out on X-ray Single Crystal Diffractometer (Bruker D8 Venture).

4.1.1. General procedures for the synthesis of compounds 10, 12 and 14

To a stirred solution of started materials **9**, **11** or **13** (20 mmol, 1.0 equiv) in DMF (40mL) was added Cs_2CO_3 (30 mmol, 1.5 equiv). Then bromoacetone (26 mmol, 1.3 equiv) was added dropwise under an ice bath over a period of 60 min. The mixture was stirred and heated at 60 °C for 8 h. After cooling to room temperature, the aqueous layer was extracted with ethyl acetate (3×150 mL), and the combined organic layers were washed with brine, dried over sodium sulfate, and concentrated under reduced pressure. The residue was purified by column chromatography on silica gel (PE/EtOAc = 10:1) to afford intermediates **10**, **12** and **14**.

4.1.1.1. 1-(7-bromobenzofuran-2-yl) ethan-1-one (10)

White solid; yield: 38 %. ^1H NMR (600 MHz, CDCl_3) δ 7.65 (t, J = 7.1 Hz, 2H), 7.55 (s, 1H), 7.21 (t, J = 7.8 Hz, 1H), 2.66 (s, 3H). ESI-HRMS $[\text{M}+\text{H}]^+$ calcd for $\text{C}_{10}\text{H}_8\text{BrO}_2^+$ 238.9702, found 238.9705.

4.1.1.2. 1-(6-bromobenzofuran-2-yl) ethan-1-one (12)

White solid; yield: 42 %. ^1H NMR (600 MHz, CDCl_3) δ 7.77 (s, 1H), 7.58 (d, J = 8.4 Hz, 1H), 7.48 – 7.44 (m, 2H), 2.61 (s, 3H). ESI-HRMS $[\text{M}+\text{H}]^+$ calcd for $\text{C}_{10}\text{H}_8\text{BrO}_2^+$ 238.9702, found 238.9707.

4.1.1.3. 1-(5,7-dibromobenzofuran-2-yl)ethan-1-one (14)

White solid; yield: 35 %. ^1H NMR (600 MHz, CDCl_3) δ 7.79 (dd, J = 16.5, 1.7 Hz, 2H), 7.48 (s, 1H), 2.66 (s, 3H). ESI-HRMS $[\text{M}+\text{H}]^+$ calcd for $\text{C}_{10}\text{H}_7\text{Br}_2\text{O}_2^+$ 318.8787, found 318.8790.

4.1.2. General procedures for the synthesis of compounds **15**, **A1-A17** and **B1-B7**

To a solution of compounds **10**, **12** or **14** (0.84 mmol, 1.0 equiv) in toluene (10 mL) were added the corresponding aniline (0.76 mmol, 0.9 equiv), Cs_2CO_3 (1.176 mmol, 1.4 equiv), BINAP (0.084 mmol, 0.1 equiv), and $\text{Pd}(\text{OAc})_2$ (0.084 mmol, 0.1 equiv) at room temperature. The reaction mixture was allowed to stir at 120 °C for about 10 h and monitored by TLC. After cooling to room temperature, diluted with ethyl acetate, washed with brine and dried with sodium sulfate. The solution was concentrated *in vacuo*, then loaded on silica gel, and purified by silica gel chromatography with petroleum/ethyl acetate as eluent to give the compounds **15**, **A1-A17** and **B1-B7**.

4.1.2.1. 1-(5-bromo-7-((3,5-dimethoxyphenyl)amino)benzofuran-2-yl)ethan-1-one (**15**)

Yellow solid; yield: 36 %. ^1H NMR (600 MHz, CDCl_3) δ 7.46 (d, J = 1.6 Hz, 1H), 7.42 (s, 1H), 7.31 (d, J = 1.7 Hz, 1H), 6.39 (d, J = 2.1 Hz, 2H), 6.33 (s, 1H), 6.21 (t, J = 2.1 Hz, 1H), 3.80 (s, 6H), 2.61 (s, 3H). ^{13}C NMR (150 MHz, CDCl_3) δ 188.02, 161.69, 152.75, 144.61, 142.17, 130.85, 128.77, 117.70, 116.05, 115.16, 113.50, 98.18, 95.15, 55.44, 26.54. ESI-HRMS $[\text{M}+\text{H}]^+$ calcd for $\text{C}_{18}\text{H}_{17}\text{BrNO}_4^+$ 390.0335, found 390.0336.

4.1.2.2. 1-(7-((3-(trifluoromethyl)phenyl)amino)benzofuran-2-yl)ethan-1-one (**A1**)

Yellow solid; yield: 57 %. ^1H NMR (600 MHz, $\text{DMSO}-d_6$) δ 8.84 (s, 1H), 7.94 (s, 1H), 7.50 – 7.42 (m, 2H), 7.37 (dd, J = 7.7, 1.0 Hz, 1H), 7.33 – 7.28 (m, 3H), 7.15 (d, J = 7.6 Hz, 1H), 3.34 (s, 3H). ^{13}C NMR (150 MHz, $\text{DMSO}-d_6$) δ 188.31, 152.42, 147.46, 144.78, 130.60, 128.84, 128.10, 125.25, 119.92, 117.83, 117.29, 116.06, 115.27, 112.73, 112.70, 26.85. ESI-HRMS $[\text{M}+\text{H}]^+$ calcd for $\text{C}_{17}\text{H}_{13}\text{F}_3\text{NO}_2^+$ 320.0893, found 320.0898.

4.1.2.3. 1-(7-(phenylamino)benzofuran-2-yl)ethan-1-one (**A2**)

Yellow solid; yield: 36 %. ^1H NMR (600 MHz, CDCl_3) δ 7.53 (s, 1H), 7.36 – 7.31 (m, 3H), 7.17-7.25 (m, 4H), 7.03 (t, J = 7.4 Hz, 1H), 6.29 (s, 1H), 2.62 (s, 3H). ^{13}C NMR (150 MHz, CDCl_3) δ 188.29, 152.23, 146.09, 141.44, 129.93, 129.44, 127.67, 124.68,

122.24, 119.15, 114.45, 114.02, 112.39, 26.49. ESI-HRMS $[M+H]^+$ calcd for $C_{16}H_{14}NO_2^+$ 252.1019, found 252.1021.

4.1.2.4. 1-(7-(m-tolylamino)benzofuran-2-yl)ethan-1-one (A3)

Yellow solid; yield: 41 %. 1H NMR (600 MHz, $CDCl_3$) δ 7.52 (s, 1H), 7.34 (dd, J = 6.6, 2.2 Hz, 1H), 7.24 – 7.18 (m, 3H), 7.04 (d, J = 7.0 Hz, 2H), 6.85 (d, J = 7.4 Hz, 1H), 6.25 (s, 1H), 2.62 (s, 3H), 2.35 (s, 3H). ^{13}C NMR (150 MHz, $CDCl_3$) δ 188.30, 152.23, 146.07, 141.37, 139.37, 130.07, 129.26, 127.64, 124.70, 123.13, 119.89, 116.26, 114.45, 113.85, 112.39, 26.51, 21.56. ESI-HRMS $[M+H]^+$ calcd for $C_{17}H_{16}NO_2^+$ 266.1176, found 266.1172.

4.1.2.5. 1-(7-((3-chlorophenyl)amino)benzofuran-2-yl)ethan-1-one (A4)

Yellow solid; yield: 39 %. 1H NMR (600 MHz, $CDCl_3$) δ 7.53 (s, 1H), 7.36 (d, J = 7.6 Hz, 1H), 7.28 (dd, J = 7.8, 0.7 Hz, 1H), 7.25 – 7.20 (m, 3H), 7.05 (dd, J = 8.1, 1.7 Hz, 1H), 6.96 (dd, J = 7.9, 1.1 Hz, 1H), 6.30 (s, 1H), 2.61 (s, 3H). ^{13}C NMR (150MHz, $CDCl_3$) δ 188.24, 152.33, 146.37, 143.10, 135.03, 130.42, 128.67, 127.89, 124.69, 121.74, 117.97, 116.48, 115.24, 114.32, 113.86, 26.49. ESI-HRMS $[M+H]^+$ calcd for $C_{16}H_{13}ClNO_2^+$ 286.0629, found 286.0624.

4.1.2.6. 1-(7-((3-methoxyphenyl)amino)benzofuran-2-yl)ethan-1-one (A5)

Yellow solid; yield: 59 %. 1H NMR (600 MHz, $CDCl_3$) δ 7.52 (s, 1H), 7.39 (dd, J = 7.4, 1.1 Hz, 1H), 7.25 – 7.17 (m, 3H), 6.81 (dd, J = 8.0, 1.7 Hz, 1H), 6.79 (t, J = 2.2 Hz, 1H), 6.58 (dd, J = 8.2, 2.2 Hz, 1H), 6.30 (s, 1H), 3.81 (s, 3H), 2.61 (s, 3H). ^{13}C NMR (150MHz, $CDCl_3$) δ 188.26, 160.67, 152.22, 146.17, 142.82, 130.18, 129.60, 127.67, 124.68, 114.46, 114.25, 113.02, 111.38, 107.38, 104.71, 55.28, 26.49. ESI-HRMS $[M+H]^+$ calcd for $C_{17}H_{16}NO_3^+$ 282.1125, found 282.1126.

4.1.2.7. 1-(7-((3-fluorophenyl)amino)benzofuran-2-yl)ethan-1-one (A6)

Yellow solid; yield: 48 %. 1H NMR (600 MHz, $CDCl_3$) δ 7.55 (s, 1H), 7.41 (dd, J = 7.6, 1.0 Hz, 1H), 7.32 – 7.28 (m, 2H), 7.22-7.26 (m, 1H), 6.99 – 6.92 (m, 2H), 6.74 – 6.68 (m, 1H), 6.35 (s, 1H), 2.64 (s, 3H). ^{13}C NMR (150 MHz, $CDCl_3$) δ 188.23, 164.46, 162.84, 152.31, 146.39, 143.56, 130.61, 128.70, 127.87, 124.67, 115.21, 114.37, 113.91, 113.86, 108.26, 105.02, 26.48. ESI-HRMS $[M+H]^+$ calcd for $C_{16}H_{13}FNO_2^+$ 270.0925, found 270.0924.

4.1.2.8. 3-((2-acetylbenzofuran-7-yl)amino)benzonitrile (A7)

Yellow solid; yield: 38 %. ^1H NMR (600 MHz, CDCl_3) δ 7.54 (s, 1H), 7.43 (s, 1H), 7.32–7.39 (m, 4H), 7.28 – 7.26 (m, 1H), 7.24 (d, J = 8.5 Hz, 1H), 6.40 (s, 1H), 2.60 (s, 3H). ^{13}C NMR (150 MHz, CDCl_3) δ 188.14, 152.45, 146.74, 143.03, 130.30, 128.18, 127.68, 124.78, 124.71, 122.01, 119.97, 118.81, 116.42, 115.00, 114.30, 113.30, 26.49. ESI-HRMS $[\text{M}+\text{H}]^+$ calcd for $\text{C}_{17}\text{H}_{13}\text{N}_2\text{O}_2^+$ 277.0972, found 277.0972.

4.1.2.9. 1-(7-(p-tolylamino)benzofuran-2-yl)ethan-1-one (A8)

Yellow solid; yield: 39 %. ^1H NMR (600 MHz, CDCl_3) δ 7.52 (s, 1H), 7.22–7.25 (m, 1H), 7.18 – 7.14 (m, 6H), 6.21 (s, 1H), 2.62 (s, 3H), 2.34 (s, 3H). ^{13}C NMR (150 MHz, CDCl_3) δ 188.27, 152.16, 145.79, 138.60, 132.18, 130.72, 129.96, 127.53, 124.71, 120.08, 114.53, 113.30, 111.42, 26.48, 20.79. ESI-HRMS $[\text{M}+\text{H}]^+$ calcd for $\text{C}_{17}\text{H}_{16}\text{NO}_2^+$ 266.1176, found 266.1177.

4.1.2.10. 1-(7-((4-methoxyphenyl)amino)benzofuran-2-yl)ethan-1-one (A9)

Yellow solid; yield: 39 %. ^1H NMR (600 MHz, CDCl_3) δ 7.51 (s, 1H), 7.21 – 7.17 (m, 2H), 7.13 – 7.11 (m, 2H), 7.06–7.08 (m, 1H), 6.93 – 6.89 (m, 2H), 6.13 (s, 1H), 3.82 (s, 3H), 2.61 (s, 3H). ^{13}C NMR (150 MHz, CDCl_3) δ 188.27, 155.95, 152.14, 145.42, 133.98, 131.84, 127.43, 124.77, 123.15, 114.73, 114.55, 112.68, 110.40, 55.56, 26.46. ESI-HRMS $[\text{M}+\text{H}]^+$ calcd for $\text{C}_{17}\text{H}_{16}\text{NO}_3^+$ 282.1125, found 282.1134.

4.1.2.11. 1-(7-((4-(trifluoromethyl)phenyl)amino)benzofuran-2-yl)ethan-1-one (A10)

Light yellow solid; yield: 57 %. ^1H NMR (600 MHz, CDCl_3) δ 7.54 (t, J = 4.2 Hz, 3H), 7.43 (d, J = 7.7 Hz, 1H), 7.34 (d, J = 7.8 Hz, 1H), 7.27 – 7.25 (m, 1H), 7.22 (d, J = 8.5 Hz, 2H), 6.45 (s, 1H), 2.61 (s, 3H). ^{13}C NMR (150 MHz, CDCl_3) δ 188.17, 152.44, 146.83, 145.18, 128.10, 127.86, 126.76, 126.74, 124.65, 116.74, 116.19, 115.13, 114.30, 26.49. ESI-HRMS $[\text{M}+\text{H}]^+$ calcd for $\text{C}_{17}\text{H}_{13}\text{F}_3\text{NO}_2^+$ 320.0893, found 320.0893.

4.1.2.12. 1-(7-((4-fluorophenyl)amino)benzofuran-2-yl)ethan-1-one (A11)

Yellow solid; yield: 46 %. ^1H NMR (600 MHz, CDCl_3) δ 7.52 (s, 1H), 7.18 (d, J = 10.3 Hz, 5H), 7.05 (t, J = 7.8 Hz, 2H), 6.20 (s, 1H), 2.61 (s, 3H). ^{13}C NMR (150 MHz, CDCl_3) δ 188.23, 159.48, 157.88, 152.21, 145.73, 137.25, 130.65, 127.64, 124.73, 121.88, 121.83, 116.19, 116.04, 114.52, 113.74, 111.45, 26.47. ESI-HRMS $[\text{M}+\text{H}]^+$ calcd for $\text{C}_{16}\text{H}_{13}\text{FNO}_2^+$ 270.0925, found 270.0933.

4.1.2.13. 1-(7-((4-fluoro-3-methoxyphenyl)amino)benzofuran-2-yl)ethan-1-one (A12)

Yellow solid; yield: 59 %. ^1H NMR (600 MHz, CDCl_3) δ 7.53 (s, 1H), 7.23 – 7.18 (m, 3H), 7.04 (dd, J = 11.0, 8.6 Hz, 1H), 6.85 (dd, J = 7.4, 2.6 Hz, 1H), 6.78 – 6.74 (m, 1H), 6.22 (s, 1H), 3.88 (s, 3H), 2.62 (s, 3H). ^{13}C NMR (150 MHz, CDCl_3) δ 188.21, 152.19, 145.78, 137.66, 130.45, 127.65, 124.75, 116.47, 116.34, 114.60, 113.86, 111.96, 111.91, 111.75, 106.25, 56.30, 26.48. ESI-HRMS $[\text{M}+\text{H}]^+$ calcd for $\text{C}_{17}\text{H}_{15}\text{FNO}_3^+$ 300.1030, found 300.1024.

4.1.2.14. 1-(7-((3-methoxy-4-methylphenyl)amino)benzofuran-2-yl)ethan-1-one (A13)

Yellow solid; yield: 57 %. ^1H NMR (600 MHz, CDCl_3) δ 7.52 (s, 1H), 7.30 (t, J = 4.4 Hz, 1H), 7.17 (d, J = 4.4 Hz, 2H), 7.08 (d, J = 7.9 Hz, 1H), 6.77 (dd, J = 7.9, 1.4 Hz, 1H), 6.73 (s, 1H), 6.28 (s, 1H), 3.82 (s, 3H), 2.62 (s, 3H), 2.20 (s, 3H). ^{13}C NMR (150 MHz, CDCl_3) δ 188.27, 158.41, 152.13, 145.81, 140.10, 130.99, 130.66, 127.53, 124.75, 120.97, 114.63, 113.35, 111.63, 111.51, 102.91, 55.36, 26.47, 15.68. ESI-HRMS $[\text{M}+\text{H}]^+$ calcd for $\text{C}_{18}\text{H}_{18}\text{NO}_3^+$ 296.1281, found 296.1287.

4.1.2.15. 1-(7-((4-chloro-3-methoxyphenyl)amino)benzofuran-2-yl)ethan-1-one (A14)

Yellow solid; yield: 43 %. ^1H NMR (600 MHz, CDCl_3) δ 7.54 (s, 1H), 7.33 (d, J = 7.6 Hz, 1H), 7.28 (d, J = 8.2 Hz, 1H), 7.25 (s, 1H), 7.21 (t, J = 7.7 Hz, 1H), 6.78 (d, J = 8.2 Hz, 2H), 6.33 (s, 1H), 3.89 (s, 3H), 2.62 (s, 3H). ^{13}C NMR (150 MHz, CDCl_3) δ 188.19, 155.65, 152.23, 146.17, 141.47, 130.57, 129.35, 127.79, 124.72, 115.22, 114.66, 114.58, 112.99, 111.34, 103.44, 56.15, 26.48. ESI-HRMS $[\text{M}+\text{H}]^+$ calcd for $\text{C}_{17}\text{H}_{15}\text{ClNO}_3^+$ 316.0735, found 316.0732.

4.1.2.16. Synthesis of 1-(7-((3,4-dimethoxyphenyl)amino)benzofuran-2-yl)ethan-1-one (A15).

Yellow solid; yield: 57 %. ^1H NMR (600 MHz, CDCl_3) δ 7.53 (s, 1H), 7.15 (s, 3H), 6.87 (d, J = 9.1 Hz, 1H), 6.82 (d, J = 6.1 Hz, 2H), 6.19 (s, 1H), 3.89 (d, J = 14.1 Hz, 6H), 2.62 (s, 3H). ^{13}C NMR (150 MHz, CDCl_3) δ 188.27, 152.13, 149.65, 145.50, 145.39, 134.46, 131.56, 127.47, 124.80, 114.63, 113.19, 112.89, 112.00, 110.74, 106.16, 56.24, 55.95, 26.46. ESI-HRMS $[\text{M}+\text{H}]^+$ calcd for $\text{C}_{18}\text{H}_{18}\text{NO}_4^+$ 312.1230, found 312.1230.

4.1.2.17. 1-(7-((4-hydroxy-3-methoxyphenyl)amino)benzofuran-2-yl)ethan-1-one (A16)

Orange solid; yield: 43 %. ^1H NMR (600 MHz, CDCl_3) δ 7.52 (s, 1H), 7.15 – 7.12 (m, 2H), 7.08 (dd, J = 6.4, 2.5 Hz, 1H), 6.91 (d, J = 8.1 Hz, 1H), 6.82 – 6.78 (m, 2H), 6.13 (s, 1H), 5.46 (s, 1H), 3.88 (s, 3H), 2.62 (s, 3H). ^{13}C NMR (150 MHz, CDCl_3) δ 188.27, 152.11, 146.98, 145.37, 142.07, 133.55, 131.90, 127.42, 124.81, 114.84, 114.77, 114.63, 112.68, 110.47, 105.90, 56.00, 26.46. ESI-HRMS $[\text{M}+\text{H}]^+$ calcd for $\text{C}_{17}\text{H}_{16}\text{NO}_4^+$ 298.1074, found 298.1072.

4.1.2.18. 1-(7-((3,5-dimethoxyphenyl)amino)benzofuran-2-yl)ethan-1-one (A17)

Light yellow solid; yield: 54 %. ^1H NMR (600 MHz, CDCl_3) δ 7.52 (s, 1H), 7.42 (d, J = 7.4 Hz, 1H), 7.18-7.24 (m, 2H), 6.39 (d, J = 1.6 Hz, 2H), 6.31 (s, 1H), 6.15 (s, 1H), 3.79 (s, 6H), 2.62 (s, 3H). ^{13}C NMR (150 MHz, CDCl_3) δ 188.27, 161.62, 152.19, 146.26, 143.46, 129.36, 127.67, 124.70, 114.53, 114.42, 113.59, 97.06, 94.09, 55.37, 26.49. ESI-HRMS $[\text{M}+\text{H}]^+$ calcd for $\text{C}_{18}\text{H}_{18}\text{NO}_4^+$ 312.1230, found 312.1230.

4.1.2.19. 1-(6-((3-(trifluoromethyl)phenyl)amino)benzofuran-2-yl)ethan-1-one (B1)

yellow solid; yield: 52 %. ^1H NMR (600 MHz, CDCl_3) δ 7.60 (d, J = 8.5 Hz, 1H), 7.46 (s, 1H), 7.42 (t, J = 7.9 Hz, 1H), 7.37 (s, 1H), 7.31 (d, J = 8.1 Hz, 1H), 7.28 (s, 1H), 7.24 (d, J = 7.7 Hz, 1H), 7.02 (dd, J = 8.5, 1.9 Hz, 1H), 6.12 (s, 1H), 2.58 (s, 3H). ^{13}C NMR (150 MHz, CDCl_3) δ 187.88, 157.29, 152.30, 143.48, 142.69, 130.07, 124.15, 121.31, 121.26, 118.41, 118.38, 116.21, 114.80, 114.77, 113.85, 99.64, 26.24. ESI-HRMS $[\text{M}+\text{H}]^+$ calcd for $\text{C}_{17}\text{H}_{13}\text{F}_3\text{NO}_2^+$ 320.0893, found 320.0892.

4.1.2.20. 1-(6-(phenylamino)benzofuran-2-yl)ethan-1-one (B2)

Light yellow solid; yield: 74 %. ^1H NMR (600 MHz, CDCl_3) δ 7.53 (d, J = 8.5 Hz, 1H), 7.43 (s, 1H), 7.33 (t, J = 7.9 Hz, 2H), 7.24 (s, 1H), 7.18 (d, J = 7.7 Hz, 2H), 7.04 (t, J = 7.4 Hz, 1H), 6.97 (dd, J = 8.5, 1.9 Hz, 1H), 6.02 (s, 1H), 2.56 (s, 3H). ^{13}C NMR (150 MHz, CDCl_3) δ 187.74, 157.61, 151.94, 145.03, 141.64, 129.55, 123.88, 122.56, 120.23, 119.44, 115.58, 114.03, 98.01, 26.17. ESI-HRMS $[\text{M}+\text{H}]^+$ calcd for $\text{C}_{16}\text{H}_{14}\text{NO}_2^+$ 252.1019, found 252.1009.

4.1.2.21. 1-(6-(*m*-tolylamino)benzofuran-2-yl)ethan-1-one (B3)

Yellow solid; yield: 54 %. ^1H NMR (600 MHz, CDCl_3) δ 7.53 (d, J = 8.5 Hz, 1H), 7.43 (d, J = 0.8 Hz, 1H), 7.25 (s, 1H), 7.21 (t, J = 7.7 Hz, 1H), 7.01 (s, 1H), 6.99 – 6.94 (m, 2H), 6.86 (d, J = 7.5 Hz, 1H), 6.00 (s, 1H), 2.56 (s, 3H), 2.34 (s, 3H). ^{13}C NMR (150

MHz, CDCl₃) δ 187.69, 157.63, 151.82, 145.14, 141.50, 139.48, 129.36, 123.83, 123.41, 120.06, 120.03, 116.53, 115.61, 114.16, 97.84, 26.13, 21.52. ESI-HRMS [M+H]⁺ calcd for C₁₇H₁₆NO₂⁺ 266.1176, found 266.1164.

4.1.2.22. 1-(6-((4-(trifluoromethyl)phenyl)amino)benzofuran-2-yl)ethan-1-one (B4)

Yellow solid; yield: 48 %. ¹H NMR (600 MHz, CDCl₃) δ 7.61 (d, *J* = 8.5 Hz, 1H), 7.53 (d, *J* = 8.5 Hz, 2H), 7.46 (s, 1H), 7.35 (s, 1H), 7.17 (d, *J* = 8.5 Hz, 2H), 7.07 (dd, *J* = 8.5, 1.9 Hz, 1H), 6.21 (s, 1H), 2.58 (s, 3H). ¹³C NMR (150 MHz, CDCl₃) δ 187.91, 157.09, 152.55, 145.48, 142.61, 126.88, 126.85, 124.10, 121.86, 116.96, 116.74, 113.55, 100.96, 26.28. ESI-HRMS [M+H]⁺ calcd for C₁₇H₁₃F₃NO₂⁺ 320.0893, found 320.0900.

4.1.2.23. 1-(6-(*p*-tolylamino)benzofuran-2-yl)ethan-1-one (B5)

Orange solid; yield: 54 %. ¹H NMR (600 MHz, CDCl₃) δ 7.51 (d, *J* = 8.5 Hz, 1H), 7.42 (s, 1H), 7.17 – 7.13 (m, 3H), 7.09 (d, *J* = 8.3 Hz, 2H), 6.91 (dd, *J* = 8.5, 2.0 Hz, 1H), 5.92 (s, 1H), 2.55 (s, 3H), 2.34 (s, 3H). ¹³C NMR (150 MHz, CDCl₃) δ 187.65, 157.76, 151.75, 145.89, 138.78, 132.62, 130.07, 123.81, 120.42, 119.72, 115.03, 114.12, 97.04, 26.12, 20.81. ESI-HRMS [M+H]⁺ calcd for C₁₇H₁₅NO₂⁺ 266.1176, found 266.1173.

4.1.2.24. 1-(6-((4-fluoro-3-methylphenyl)amino)benzofuran-2-yl)ethan-1-one (B6)

Yellow solid; yield: 73 %. ¹H NMR (600 MHz, CDCl₃) δ 7.51 (d, *J* = 8.5 Hz, 1H), 7.42 (s, 1H), 7.10 (s, 1H), 7.02 (d, *J* = 5.1 Hz, 1H), 7.00 – 6.93 (m, 2H), 6.88 (dd, *J* = 8.5, 1.7 Hz, 1H), 5.85 (s, 1H), 2.55 (s, 3H), 2.27 (s, 3H). ¹³C NMR (150 MHz, CDCl₃) δ 187.63, 157.71, 151.78, 146.07, 137.00, 123.92, 123.89, 123.86, 119.78, 119.72, 115.85, 115.70, 114.85, 114.13, 96.89, 26.12, 14.75. ESI-HRMS [M+H]⁺ calcd for C₁₇H₁₅FNO₂⁺ 284.1081, found 284.1077.

4.1.2.25. 1-(6-((3-fluoro-5-methylphenyl)amino)benzofuran-2-yl)ethan-1-one (B7)

Yellow solid; yield: 63 %. ¹H NMR (600 MHz, CDCl₃) δ 7.56 (d, *J* = 8.5 Hz, 1H), 7.44 (d, *J* = 0.6 Hz, 1H), 7.29 (s, 1H), 6.99 (dd, *J* = 8.5, 2.0 Hz, 1H), 6.72 (s, 1H), 6.68 (dd, *J* = 10.5, 2.0 Hz, 1H), 6.52 (d, *J* = 9.3 Hz, 1H), 6.05 (s, 1H), 2.57 (s, 3H), 2.32 (s, 3H). ¹³C NMR (150 MHz, CDCl₃) δ 187.81, 164.43, 157.35, 152.14, 143.88, 143.40, 141.36, 123.95, 120.87, 116.24, 114.63, 113.91, 109.40, 102.57, 99.34, 26.19, 21.56. ESI-HRMS [M+H]⁺ calcd for C₁₇H₁₅FNO₂⁺ 284.1081, found 284.1076.

4.1.3. General procedures for the synthesis of compounds **C1-C6**

To a Schlenk flask was added the corresponding boronic acid (0.154 mmol, 1.5 equiv), compound **15** (40 mg, 0.103 mmol, 1.0 equiv), Pd(dppf)Cl₂ (7.54 mg, 0.0103 mmol, 0.1 equiv), K₂CO₃ (28.4 mg, 0.206 mmol, 2.0 equiv), then diluted with H₂O (0.1 mL) and DMF (3 mL) under nitrogen atmosphere. The reaction mixture was refluxed at 100 °C for 8 h. After cooling to room temperature, the mixture was quenched with water and extracted with ethyl acetate. The organic solvent was removed under reduced pressure and the residue was purified by silica-gel column chromatography to give the compounds **C1-C6**.

4.1.3.1. 1-(7-((3,5-dimethoxyphenyl)amino)-5-phenylbenzofuran-2-yl)ethan-1-one (**C1**)

Yellow solid; yield: 76 %. ¹H NMR (600 MHz, CDCl₃) δ 7.64 (d, *J* = 1.2 Hz, 1H), 7.57 (d, *J* = 6.0 Hz, 3H), 7.44 (t, *J* = 7.6 Hz, 2H), 7.40 (d, *J* = 1.3 Hz, 1H), 7.35 (t, *J* = 7.4 Hz, 1H), 6.44 (d, *J* = 2.1 Hz, 2H), 6.32 (s, 1H), 6.17 (t, *J* = 2.0 Hz, 1H), 3.79 (s, 6H), 2.64 (s, 3H). ¹³C NMR (150 MHz, CDCl₃) δ 188.21, 161.66, 152.71, 145.87, 143.32, 141.24, 138.70, 129.38, 128.80, 128.09, 127.42, 127.30, 114.65, 113.40, 112.81, 97.26, 94.34, 55.38, 26.52. ESI-HRMS [M+H]⁺ calcd for C₂₄H₂₂NO₄⁺ 388.1543, found 388.1550.

4.1.3.2. 1-(7-((3,5-dimethoxyphenyl)amino)-5-(thiophen-2-yl)benzofuran-2-yl)ethan-1-one (**C2**)

Yellow solid; yield: 84 %. ¹H NMR (600 MHz, CDCl₃) δ 7.70 (d, *J* = 1.2 Hz, 1H), 7.52 (s, 1H), 7.43 (d, *J* = 1.3 Hz, 1H), 7.27 (s, 1H), 7.25 (s, 1H), 7.07 (dd, *J* = 4.9, 3.7 Hz, 1H), 6.44 (d, *J* = 2.1 Hz, 2H), 6.33 (s, 1H), 6.18 (t, *J* = 2.0 Hz, 1H), 3.80 (s, 6H), 2.63 (s, 3H). ¹³C NMR (150 MHz, CDCl₃) δ 188.14, 161.68, 152.80, 145.76, 144.35, 143.03, 131.63, 129.55, 128.13, 128.06, 124.83, 123.28, 114.43, 111.90, 111.37, 97.18, 94.72, 55.42, 26.52. ESI-HRMS [M+H]⁺ calcd for C₂₂H₂₀NO₄S⁺ 394.1108, found 394.1120.

4.1.3.3. 1-(5-(cyclohex-1-en-1-yl)-7-((3,5-dimethoxyphenyl)amino) benzofuran-2-yl)ethan-1-one (**C3**)

Yellow solid; yield: 74 %. ¹H NMR (600 MHz, CDCl₃) δ 7.50 – 7.47 (m, 2H), 7.20 (d, *J* = 1.3 Hz, 1H), 6.39 (d, *J* = 2.1 Hz, 2H), 6.23 (s, 1H), 6.14 (t, *J* = 2.1 Hz, 1H), 6.07 – 6.04 (m, 1H), 3.79 (s, 6H), 2.60 (s, 3H), 2.43 – 2.39 (m, 2H), 2.20-2.18 (m, 2H), 1.81

– 1.76 (m, 2H), 1.68-1.64 (m, 2H). ^{13}C NMR (150 MHz, CDCl_3) δ 188.24, 161.61, 152.49, 145.73, 143.71, 140.26, 136.55, 128.49, 127.63, 125.27, 114.70, 112.26, 110.79, 96.74, 94.06, 55.36, 27.99, 26.46, 25.88, 23.07, 22.08. ESI-HRMS $[\text{M}+\text{H}]^+$ calcd for $\text{C}_{24}\text{H}_{26}\text{NO}_4^+$ 392.1856, found 392.1862.

4.1.3.4. 1-(7-((3,5-dimethoxyphenyl)amino)-5-(furan-2-yl)benzofuran-2-yl)ethan-1-one (C4)

Yellow solid; yield: 77 %. ^1H NMR (600 MHz, CDCl_3) δ 7.75 (d, $J = 1.1$ Hz, 1H), 7.53 – 7.51 (m, 2H), 7.46 (d, $J = 1.0$ Hz, 1H), 6.60 (d, $J = 3.2$ Hz, 1H), 6.47 (dd, $J = 3.3, 1.8$ Hz, 1H), 6.43 (d, $J = 2.1$ Hz, 2H), 6.32 (s, 1H), 6.18 (t, $J = 2.1$ Hz, 1H), 3.80 (s, 6H), 2.62 (s, 3H). ^{13}C NMR (150 MHz, CDCl_3) δ 188.16, 161.69, 153.77, 152.76, 145.76, 143.20, 142.11, 129.50, 128.15, 128.01, 114.58, 111.73, 109.87, 109.42, 104.97, 97.22, 94.57, 55.42, 26.52. ESI-HRMS $[\text{M}+\text{H}]^+$ calcd for $\text{C}_{22}\text{H}_{20}\text{NO}_5^+$ 378.1336, found 378.1338.

4.1.3.5. 1-(5-(3,6-dihydro-2H-pyran-4-yl)-7-((3,5-dimethoxyphenyl)amino)benzofuran-2-yl)ethan-1-one (C5)

Yellow solid; yield: 76 %. ^1H NMR (600 MHz, CDCl_3) δ 7.50 (s, 2H), 7.20 (s, 1H), 6.39 (d, $J = 1.7$ Hz, 2H), 6.26 (s, 1H), 6.16 (s, 1H), 6.07 (s, 1H), 4.32 (d, $J = 2.5$ Hz, 2H), 3.94 (t, $J = 5.4$ Hz, 2H), 3.79 (s, 6H), 2.61 (s, 3H), 2.54 (d, $J = 1.3$ Hz, 2H). ^{13}C NMR (150 MHz, CDCl_3) δ 188.18, 161.66, 152.65, 145.89, 143.41, 137.80, 134.11, 128.98, 127.74, 122.83, 114.56, 111.25, 110.53, 97.04, 94.20, 65.85, 64.45, 55.38, 27.73, 26.49. ESI-HRMS $[\text{M}+\text{H}]^+$ calcd for $\text{C}_{23}\text{H}_{24}\text{NO}_5^+$ 394.1649, found 394.1658.

4.1.3.6. 1-(7-((3,5-dimethoxyphenyl)amino)-5-(1-methyl-1H-pyrazol-5-yl)benzofuran-2-yl)ethan-1-one (C6)

Yellow solid; yield: 81 %. ^1H NMR (600 MHz, CDCl_3) δ 7.55 (s, 1H), 7.51 (s, 1H), 7.40 (s, 1H), 7.22 (s, 1H), 6.40 (s, 3H), 6.29 (s, 1H), 6.18 (s, 1H), 3.90 (s, 3H), 3.79 (s, 6H), 2.64 (s, 3H). ^{13}C NMR (150 MHz, CDCl_3) δ 188.09, 161.70, 152.89, 145.71, 143.46, 142.63, 138.52, 129.85, 127.77, 127.68, 114.29, 114.26, 113.43, 106.28, 97.90, 94.59, 55.38, 37.50, 26.55. ESI-HRMS $[\text{M}+\text{H}]^+$ calcd for $\text{C}_{22}\text{H}_{22}\text{N}_3\text{O}_4^+$ 392.1605, found 392.1613.

4.1.4. 1-(7-((3,5-dimethoxyphenyl)amino)-5-morpholinobenzofuran-2-yl)ethan-1-one (C7)

A mixture of compound **15** (40 mg, 0.103 mmol, 1.0 equiv), Morpholine (17.9 mg, 0.206 mmol, 2.0 equiv), K₂CO₃ (28.4 mg, 0.206 mmol, 2.0 equiv), CuI (3.9 mg, 0.206 mmol, 20 mol %) and L-proline (2.4 mg, 0.0206 mmol, 20 mol %) in 2 mL of DMSO was heated to 90 °C and stirred for 12 h under nitrogen environment. Upon completion, the reaction mixture was cooled to room temperature, filtered and washed with EtOAc. The combined organic layers were washed with brine, dried over Na₂SO₄, and concentrated *in vacuo*. The removal of the solvent yielded a residue that was purified by silica gel column chromatography (petroleum: EtOAc = 4:1 as eluent) on silica gel to afford pure product. Yellow solid; yield: 78 %. ¹H NMR (600 MHz, CDCl₃) δ 7.43 (s, 1H), 7.12 (d, *J* = 2.0 Hz, 1H), 6.65 (d, *J* = 1.9 Hz, 1H), 6.38 (d, *J* = 2.1 Hz, 2H), 6.27 (s, 1H), 6.15 (t, *J* = 2.1 Hz, 1H), 3.86 (t, *J* = 4.62 Hz, 4H), 3.78 (s, 6H), 3.12 – 3.10 (m, 4H), 2.59 (s, 3H). ¹³C NMR (150 MHz, CDCl₃) δ 188.18, 161.64, 152.61, 149.71, 143.38, 142.19, 129.46, 127.99, 114.45, 105.99, 99.83, 97.21, 94.19, 66.97, 55.36, 50.97, 26.41. ESI-HRMS [M+H]⁺ calcd for C₂₂H₂₅N₂O₅⁺ 397.1758, found 397.1771.

4.2. Biological evaluation

4.2.1. Cell lines culture

Cancer cell lines (MDA-MB-468, HepG2, MDA-MB-231, A549, U251, HCT116) were purchased from the Cell Bank of Shanghai Institute of Biochemistry and Cell Biology, Chinese Academy of Sciences (Shanghai, China). Cells were cultured in corresponding cell culture medium (MDA-MB-468, MDA-MB-231: DMEM/F-12, Biological Industries, Beit Haemek, Israel; U251, HepG2: DMEM, Biological Industries, Beit Haemek, Israel; HCT116, A549: RPMI1640, Biological Industries, Beit Haemek, Israel) supplemented with 10 % fetal bovine serum (FBS, Gibco) and 1 % penicillin/streptomycin. cells were incubated at 37 °C in a humidified atmosphere containing 5 % CO₂ and Medium was replaced every 2 d. When cells were 80–90 % confluent and passaged at a culture ratio of 1:1 and cells in the logarithmic growth phase were assessed for further experiments.

4.2.2. *In vitro* cell growth inhibitory activity assays

Cancer cells were plated in 96-well transparent plates at a density of 6000-8000/well. After overnight incubation, Test compounds were added onto triplicate wells with different concentrations for 48 h at 37 °C and 0.1 % DMSO for control. After incubation and removing the cell culture medium, 10 % Cell Counting Kit-8 (CCK-8, APEX BIO, Houston, USA) solution (100 µL) was added to each well and re-incubated for 4 h. Then the absorbance was measured on a microplate spectrophotometer (MK3, Thermo, Germany) at 450 nm. The cytotoxic activity was expressed as the IC₅₀ values and all experiments were conducted in triplicate.

4.2.3. *Western blot analysis*

MDA-MB-468 cells were seeded (10×10^5 cells) in each of 60 mm cell culture dish (Corning). Cells were incubated with various concentrations of compound **C6** for 24 h, then washed with cold-ice PBS for 2 times and 100 µL of lysis buffer containing 1 % protease and phosphatase inhibitors (Beyotime Biotechnology) for 10 min. Then centrifuged for 12000 rpm for 10 min at 4 °C to obtain the protein lysate, and BCA protein assay kit was used to measure the protein concentration. Lysates containing 40 µg of total protein were fractionated on a 10 % SDS-PAGE and wet-transferred to PVDF membranes (BioRad Laboratories, Hercules, CA). Then blocked with 5% non-fat powdered milk in TBST buffer for 2 h at room temperature and blotted with primary antibodies specific for STAT3, p-STAT3, STAT1, p-STAT1, C-Myc, Cleaved Caspase 3, Caspase 3 and GAPDH at 4 °C for overnight. The blots were washed and incubated with secondary antibodies conjugated with HRP for 1 h. Enhanced chemiluminescence (ECL, BioRad Laboratories, Hercules, CA) and bioanalytical imaging system (Azure biosystems, Inc, C600) were used for detection of target proteins.

4.2.4. *Flow cytometry analysis of apoptotic cells*

Apoptosis was determined by flow cytometry in accordance with the manufacturer's instructions. An Annexin V-FITC/PI double-staining assay was used to analyze the apoptosis. MDA-MB-468 cells at a density of 2×10^5 per well were incubated with various concentrations of compound **C6** for 48 h. Then the cells were harvested, washed, resuspending in 500 µL of binding buffer and stained with 5 µL Annexin V-FITC and

10 μ L propidium iodide at room temperature in the dark for 15 min. Finally, stained cells were detected by a flow cytometer (Beckman coulter, Inc, A00-1-1102).

4.2.5 cell cycle effect

MDA-MB-468 cells (2×10^5 cells/well) were incubated with various concentrations of compound **C6** for 24 h. The cells were harvested, collected by centrifugation, washed twice with PBS and fixed in ice-cold 70 % ethanol overnight at -20°C . The next day, cells were washed two times with PBS and resuspended in Propidium Iodide (PI)/RNase Staining Solution for 30 min at 37°C . Stained cells were analyzed by flow cytometry (Beckman coulter, Inc, A00-1-1102).

4.3. Molecular docking

Molecular docking procedure is similar to the published method.³⁶

4.4. X-ray crystal structure determination of compound **C6**

A total of 321 frames were collected. The total exposure time was 0.89 hours. The frames were integrated with the Bruker SAINT software package using a narrow-frame algorithm. The integration of the data using an orthorhombic unit cell yielded a total of 21611 reflections to a maximum θ angle of 26.48° (0.80 Å resolution), of which 4079 were independent (average redundancy 5.298, completeness = 99.5 %, $R_{\text{int}} = 9.75$ %, $R_{\text{sig}} = 6.59$ %) and 2893 (70.92 %) were greater than $2\sigma(F^2)$. The final cell constants of $a = 21.5970(12)$ Å, $b = 4.0643(3)$ Å, $c = 22.7339(11)$ Å, volume = $1995.5(2)$ Å³, are based upon the refinement of the XYZ-centroids of 3441 reflections above $20\sigma(I)$ with $5.203^\circ < 2\theta < 45.45^\circ$. Data were corrected for absorption effects using the Multi-Scan method (SADABS). The ratio of minimum to maximum apparent transmission was 0.690. The calculated minimum and maximum transmission coefficients (based on crystal size) are 0.9820 and 0.9990.

The structure was solved and refined using the Bruker SHELXTL Software Package, using the space group $Pca2_1$, with $Z = 4$ for the formula unit, $\text{C}_{22}\text{H}_{21}\text{N}_3\text{O}_4$. The final anisotropic full-matrix least-squares refinement on F^2 with 271 variables converged at $R_1 = 5.60$ %, for the observed data and $wR_2 = 15.61$ % for all data. The goodness-of-fit was 1.031. The largest peak in the final difference electron density synthesis was $0.251\text{ e}^-/\text{\AA}^3$ and the largest hole was $-0.210\text{ e}^-/\text{\AA}^3$ with an RMS deviation of 0.053 e^-

/Å³. On the basis of the final model, the calculated density was 1.303 g/cm³ and F(000), 824 e⁻.

All the crystallographic parameters (excluding structure factors) of this structure have been deposited in the Cambridge Crystallographic Data Center as supplementary publication number CCDC 2018188. Copies of the data can be obtained, free of charge, on application to CCDC, 12 Union Road, Cambridge CB2 1EZ, UK [fax: +44 (0) 223 336033 or e-mail: deposit@ccdc.cam.ac.uk].

Declaration of competing interest

The authors declare that they have no known competing financial interests or personal relationships that could have appeared to influence the work reported in this paper.

Acknowledgement

Financial support was generously provided by the National Natural Science Foundation of China (Nos. 81903423 and 21871184), the Shanghai Sailing Program (19YF1449300), the Shanghai Municipal Education Commission (2019-01-07-00-10-E00072), and the Science and Technology Commission of Shanghai Municipality (18401933500).

Appendix A. Supplementary data

Supplementary data related to this article can be found at

Reference

1. Miklossy G, Hilliard TS, Turkson J. Therapeutic modulators of STAT signalling for human diseases. *Nat Rev Drug Discov.* 2013; 12(8): 611-629.
2. Page BD, Ball DP, Gunning PT. Signal transducer and activator of transcription 3 inhibitors: a patent review. *Expert Opin Ther Pat.* 2011; 21(1): 65-83.
3. Barton BE, Karras JG, Murphy TF, et al. Signal transducer and activator of transcription 3 (STAT3) activation in prostate cancer: Direct STAT3 inhibition

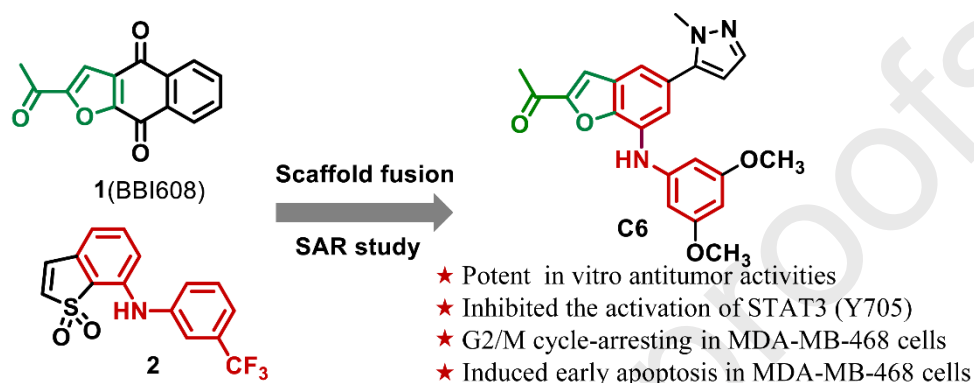
- induces apoptosis in prostate cancer lines. *Mol Cancer Ther.* 2004; 3(1): 11-20.
4. Fletcher S, Page BD, Zhang X, et al. Antagonism of the Stat3-Stat3 protein dimer with salicylic acid based small molecules. *Chem Med Chem.* 2011; 6(8): 1459-1470.
 5. Chen H, Yang Z, Ding C, et al. Discovery of potent anticancer agent HJC0416, an orally bioavailable small molecule inhibitor of signal transducer and activator of transcription 3 (STAT3). *Eur J Med Chem.* 2014; 82: 195-203.
 6. Yu H, Lee H, Herrmann A, et al. Revisiting STAT3 signalling in cancer: new and unexpected biological functions. *Nat Rev Cancer.* 2014; 14(11): 736-746.
 7. Ghoshal S, Fuchs BC, Tanabe KK. STAT3 is a key transcriptional regulator of cancer stem cell marker CD133 in HCC. *Hepatobiliary Surg Nutr.* 2016; 5(3): 201-203.
 8. Xu J, Cole DC, Chang CP, et al. Inhibition of the signal transducer and activator of transcription-3 (STAT3) signaling pathway by 4-oxo-1-phenyl-1,4-dihydroquinoline-3-carboxylic acid esters. *J Med Chem.* 2008;51(14):4115-4121.
 9. Huang W, Dong Z, Wang F, et al. A small molecule compound targeting STAT3 DNA-binding domain inhibits cancer cell proliferation, migration, and invasion. *ACS Chem Biol.* 2014; 9(5): 1188-1196.
 10. Bowman T, Garcia R, Turkson J, et al. STATs in oncogenesis. *Oncogene.* 2000; 19(21): 2474-2488.
 11. Tong M, Wang J, Jiang N, et al. Correlation between p-STAT3 overexpression and prognosis in lung cancer: A systematic review and meta-analysis. *PLoS One.* 2017; 12(8): e0182282.
 12. Beebe JD, Liu JY, Zhang JT. Two decades of research in discovery of anticancer drugs targeting STAT3, how close are we? *Pharmacol Ther.* 2018; 191: 74-91.
 13. Yu H, Jove R. The STATs of cancer--new molecular targets come of age. *Nat Rev Cancer.* 2004; 4(2): 97-105.
 14. Villarino AV, Kanno Y, Ferdinand JR, et al. Mechanisms of Jak/STAT signaling in immunity and disease. *J Immunol.* 2015; 194(1): 21-27.
 15. Johnson DE, O'Keefe RA, Grandis JR. Targeting the IL-6/JAK/STAT3 signalling axis in cancer. *Nat Rev Clin Oncol.* 2018; 15(4): 234-248.

16. Wang Y, Shen Y, Wang S, et al. The role of STAT3 in leading the crosstalk between human cancers and the immune system. *Cancer Lett.* 2018; 415: 117-128.
17. Kusaba T, Nakayama T, Yamazumi K, et al. Activation of STAT3 is a marker of poor prognosis in human colorectal cancer. *Oncol Rep.* 2006; 15(6): 1445-1451.
18. Chen Y, Wang J, Wang X, et al. STAT3, a Poor Survival Predictor, Is Associated with Lymph Node Metastasis from Breast Cancer. *J Breast Cancer.* 2013; 16(1): 40-49.
19. Macha MA, Matta A, Kaur J, et al. Prognostic significance of nuclear pSTAT3 in oral cancer. *Head Neck.* 2011; 33(4): 482-489.
20. Q. Huang, Y. Zhong, H. Dong, Q. Zheng, S. Shi, K. Zhu, X. Qu, W. Hu, X. Zhang, Y. Wang, Revisiting signal transducer and activator of transcription 3 (STAT3) as an anticancer target and its inhibitor discovery: Where are we and where should we go? *Eur. J. Med. Chem.* 2020; 187: 111922.
21. P. Shih. Revisiting the development of small molecular inhibitors that directly target the signal transducer and activator of transcription 3 (STAT3) domains. *Life Sci.* 2020; 242: 117241.
22. Li Y, Rogoff HA, Keates S, et al. Suppression of cancer relapse and metastasis by inhibiting cancer stemness. *Proc Natl Acad Sci U S A.* 2015; 112(6): 1839-1844.
23. Zhang W, Ma T, Li S, et al. Antagonizing STAT3 activation with benzo[b]thiophene 1,1-dioxide based small molecules. *Eur J Med Chem.* 2017; 125: 538-550.
24. Yu W, Xiao H, Lin J, et al. Discovery of novel STAT3 small molecule inhibitors via in silico site-directed fragment-based drug design. *J Med Chem.* 2013; 56(11): 4402-4412.
25. Schust J, Sperl B, Hollis A, et al. Stattic: a small-molecule inhibitor of STAT3 activation and dimerization. *Chem Biol.* 2006; 13(11): 1235-1242.
26. Lin L, Benson DM Jr, DeAngelis S, et al. A small molecule, LLL12 inhibits constitutive STAT3 and IL-6-induced STAT3 signaling and exhibits potent growth suppressive activity in human multiple myeloma cells. *Int J Cancer.* 2012; 130(6): 1459-1469.

27. Song H, Wang R, Wang S, et al. A low-molecular-weight compound discovered through virtual database screening inhibits Stat3 function in breast cancer cells. *Proc Natl Acad Sci U S A*. 2005; 102(13): 4700-4705.
28. Ren X, Duan L, He Q, et al. Identification of Niclosamide as a New Small-Molecule Inhibitor of the STAT3 Signaling Pathway. *ACS Med Chem Lett*. 2010; 1(9): 454-459.
29. Chen H, Yang Z, Ding C, et al. Discovery of potent anticancer agent HJC0416, an orally bioavailable small molecule inhibitor of signal transducer and activator of transcription 3 (STAT3). *Eur J Med Chem*. 2014; 82: 195-203.
30. <https://www.cancer.gov/about-cancer/treatment/clinical-trials/intervention/napabucasin>
31. Setoh M, Ishii N, Kono M, et al. Discovery of the first potent and orally available agonist of the orphan G-protein-coupled receptor 52. *J Med Chem*. 2014; 57(12): 5226-5237.
32. Di Santo R, Costi R, Cuzzucoli Crucitti G, et al. Design, synthesis, and structure-activity relationship of N-arylnaphthylamine derivatives as amyloid aggregation inhibitors. *J Med Chem*. 2012; 55(19): 8538-8548.
33. Markwalder JA, Seitz SP, Blat Y, et al. Identification and optimization of a novel series of indoleamine 2,3-dioxygenase inhibitors. *Bioorg Med Chem Lett*. 2017; 27(3): 582-585.
34. Ma D, Cai Q, Zhang H. Mild method for Ullmann coupling reaction of amines and aryl halides. *Org Lett*. 2003; 5(14): 2453-2455.
35. CCDC 2018188 (C6) contains the supplementary crystallographic data for this paper. These data can be obtained free of charge from The Cambridge Crystallographic Data Centre via www.ccdc.cam.ac.uk/data_request/cif.
36. Feng K, Wang F, Shi XW, et al. Design, synthesis and biological evaluation of novel potent STAT3 inhibitors based on BBI608 for cancer therapy. *Eur J Med Chem*. 2020; 201: 112428.

Identification of novel STAT3 inhibitors bearing 2-acetyl-7-phenylamino benzofuran scaffold for antitumour study

Feng Wang [#], Kai-Rui Feng [#], Jia-Ying Zhao, Jian-Wei Zhang, Xin-Wei Shi, Jian Zhou ^{*}, Dingding Gao ^{*}, Guo-Qiang Lin, and Ping Tian ^{*}



Declaration of competing interest

The authors declare that they have no known competing financial interests or personal relationships that could have appeared to influence the work reported in this paper.